Journal of Rock Mechanics and Geotechnical Engineering 18 (2026) 4108–4124

Contents lists available at ScienceDirect

Journal of Rock Mechanics and Geotechnical Engineering

journal homepage: www.jrmge.cn

Full Length Article

Effect of wet-dry cycles and physico-chemical factors on red soil-bentonite mixtures: Volumetric and hydraulic response

A.S. Devapriya, T. Thyagaraj *

Department of Civil Engineering, Indian Institute of Technology Madras, Chennai, 600 036, India

ARTICLE INFO

Article history:
Received 4 January 2025
Received in revised form
20 August 2025
Accepted 21 August 2025
Available online 8 November 2025

Keywords:
Landfill liners
Climate change adaptation
Hydraulic conductivity
Wet-dry cycles
Physico-chemical factors
Microstructure
Laboratory investigation

ABSTRACT

Landfill facilities around the world are designed to protect the environment and public health by using impermeable liner systems that isolate the waste and leachate produced from the waste. However, the functionality of liners has been reported to be significantly compromised by environmental loading due to the seasonal climatic and physico-chemical changes that alter their volume deformation and hydraulic characteristics. Bentonite admixed natural soils are employed as liner materials if they meet the hydraulic conductivity requirement in their as-compacted state. However, limited studies addressed the effects of wet-dry cycles combined with chemical contamination on the volumetric and hydraulic behaviour of bentonite admixed natural soils. In this study, Indian red soil was ameliorated with 10%, 20%, and 30% bentonite by weight, and the mixtures were subjected to alternate wetting and drying cycles using distilled water, 0.4 M NaCl, and 0.4 M $CaCl_2$ solutions. All red soil-bentonite specimens met the hydraulic conductivity design criterion of 1×10^{-7} cm/s in their as-compacted states. However, significant variation in hydraulic behaviour was observed at the end of the wet-dry cycles, particularly with chemical contamination. The microstructural examination through scanning electron microscopy (SEM) and mercury intrusion porosimetry (MIP) revealed an increase in macropores volume with wet-dry cycles and increase in the induced osmotic suction, which was found to be a key factor influencing the hydraulic conductivity.

1. Introduction

Compacted clay liners are in constant interaction with the leachate produced in the landfills, which are rich in cations such as Na^+, K^+, Ca^{2+}, and Mg^{2+} ions (Kjeldsen et al., 2002; Li et al., 2013). The difference in concentration between the soil pore fluid and the external leachate reservoir generates an osmotic gradient, inducing water migration from the pore fluid to the leachate (Mitchell and Soga, 2005; He et al., 2020). Depending on the relative concentrations, salts either diffuse into or out of the soil pore water, affecting the Diffused Double Layers (DDLs) (Rao and Thyagaraj, 2007). If the soil pore water is at a lower concentration, inward diffusion occurs, which results in the suppression of the Diffused Double Layers (DDLs). This alters the soil structure and subsequently impacts the hydraulic properties (Anandarajah, 2003; Dutta et al., 2018). Several studies have shown that the hydraulic conductivity of compacted clays increases when exposed to fluids other than water (Mishra et al., 2005; Julina and Thyagaraj, 2020; Fu et al., 2024). For example, Razakamanantsoa and Djeran-Maigre (2016) observed a tenfold increase in hydraulic conductivity when a soil–bentonite mixture was permeated with leachate compared to distilled water. This underscores the need to examine how chemical interactions influence the long-term barrier performance of compacted clay liners.

Over time, the compacted clay liners experience alternate cycles of wetting and drying, driven by seasonal moisture variations, groundwater penetration and heat and gas generated by decomposition of waste. These cycles degrade the as-compacted structure of the soils, affecting their long-term performance (Albrecht and Benson, 2001; Wan et al., 2014; He et al., 2017; Abbas et al., 2023). Compacted clays exhibit dual porosity, characterized by macropores (inter-aggregate pores) and micropores (intra aggregate pores) (Nowamooz and Masrouri, 2010; Wang and Wei, 2015;

* Corresponding author
E-mail address: ttraj@iitm.ac.in (T. Thyagaraj).

Peer review under responsibility of Institute of Rock and Soil Mechanics, Chinese Academy of Sciences.

https://doi.org/10.1016/j.jrmge.2025.08.026

Thyagaraj and Salini, 2015; Zhang et al., 2024). Wet-dry cycles alter the pore structure due to suction changes, leading to permanent deformations at the macropore level (Sun et al., 2019). Mercury Intrusion Porosimetry (MIP) tests on compacted expansive clay by Thyagaraj and Julina (2019) revealed an increase in the macropore size with repeated wet-dry cycles, particularly when exposed to 0.4 M (Mol/L) NaCl solution. This indicates a loss in the ability of clay to swell and close the macropores with exposure to wet-dry cycles and chemical contamination. Similar findings on salinization-induced macropore expansion have been reported in compacted clays (Li et al., 2020; Lin et al., 2022). Additionally, wetting and drying cycles promote microcrack formation during the drying phases, which may not fully close upon rewetting, leading to increased hydraulic conductivity in soil barriers (Yesiller et al., 2000; Li et al., 2016; Lu et al., 2025). The presence of salts exacerbates this issue by further degrading the compacted soil structure, resulting in higher hydraulic conductivity than in their as-compacted state (Lin and Benson, 2000; Lu et al., 2021; Tan et al., 2024). The interplay between cyclic moisture variations and chemical exposure could accelerate the deterioration of compacted clay liners, necessitating the targeted design modifications.

Extensive research exists on the hydraulic behavior of compacted clay liners, however, few studies explored the combined effects of wet-dry cycles and chemical exposure, particularly in natural soil-bentonite mixtures. Devapriya and Thyagaraj (2024) examined the engineering characteristics of locally available Indian red soil-bentonite mixtures for evaluating their performance under repeated wet-dry cycles. Their study analyzed mixtures containing 10%, 20%, and 30% bentonite by weight and found that while all as-compacted specimens met the hydraulic conductivity requirement ($\leq 1 \times 10^{-7}$ cm/s), the 10% bentonite specimen failed after wet-dry cycles.

This study aims to further evaluate the performance of red soil-bentonite mixtures, particularly when exposed to chemical contamination and wet-dry cycles, contributing to the development of a more resilient and effective liner material.

2. Materials and methods

2.1. Soils and chemicals used in the study

The research presented in this paper was conducted on Indian red soil collected from IIT Madras, Chennai, India. After collection of the red soil, the soil was subjected to air-drying, pulverization and sieving through the 2 mm sieve. Devapriya and Thyagaraj (2024) reported that although red soil meets the selection criteria based on index properties for compacted clay liners, its hydraulic conductivity is significantly high. To achieve the required hydraulic conductivity of $\leq 1 \times 10^{-7}$ cm/s, the red soil was modified by incorporating varying proportions of commercially procured Na-bentonite. Preliminary investigations indicated that a 10% bentonite content effectively reduced the hydraulic conductivity. To evaluate the influence of bentonite content on hydraulic performance, additional mixtures were prepared with 10%, 20%, and 30% bentonite by weight. These red soil-bentonite mixtures, hereafter referred to as R-B mixes, and are denoted as 90R-10B, 80R-20B and 70R-30B mixes. The selected bentonite contents align with reported field applications, where typical usage ranges between 3% and 30% (Sivapullaiah and Lakshmikanta, 2005; Akgun et al., 2015). Higher bentonite contents were not considered to preserve the workability of the mixtures.

To characterize the mineralogical composition, X-ray diffraction analysis (XRD) was performed. The results confirmed that kaolinite is the dominant clay mineral in the red soil, while montmorillonite is the principal clay mineral in the bentonite. Basic characterization tests were carried out and the properties are listed out in Table 1. The grain size distribution curves of the soils are presented in Fig. 1. Additionally, NaCl and $CaCl_2$ solutions of 0.4 M concentration were prepared using the sodium chloride and calcium chloride dihydrate (laboratory grade) salts for further experimental analysis.

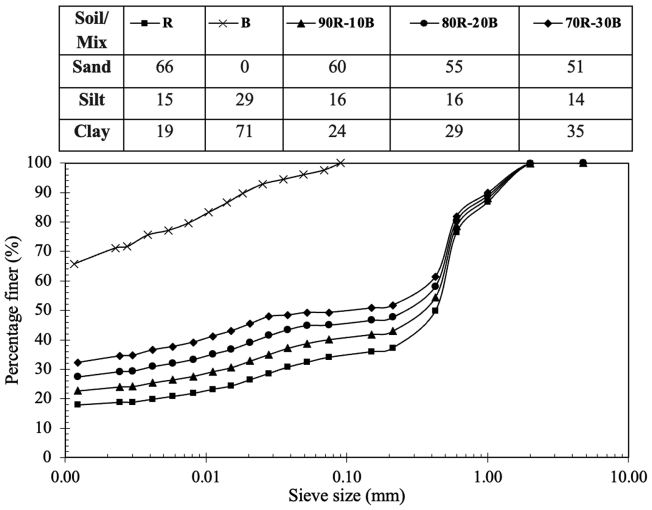

Fig. 1. Grain size distribution of red soil, bentonite and red soil-bentonite mixtures.

Table 1
Properties of red soil, bentonite and red soil-bentonite mixtures (Devapriya and Thyagaraj, 2024).

Property	Red soil (R100)	Bentonite (B)	R90-B10	R80-B20	R70-B30
Liquid limit (%)	34	224	86	113	150
Plastic limit (%)	20	48	27	35	37
Shrinkage limit (%)	15	8.4	15	13	12
Plasticity index (%)	14	176	59	78	113
Specific gravity, G_s	2.68	2.92	2.70	2.73	2.75
Grain size distribution (%)					
Sand	66	0	60	55	51
Silt	15	29	16	16	14
Clay	19	71	24	29	35
Unified Soil Classification Symbol (USCS)	SC	CH	SC	SC	SC
Maximum dry unit weight (kN/m^3)	19.4		18.75	17.6	17.15
Optimum moisture content, OMC (%)	11		12.5	15	16.5
Unconfined compressive strength (kPa)	212		230	251	272
Hydraulic conductivity (cm/s)	1.98×10^{-5}		2.69×10^{-8}	1.75×10^{-8}	1.56×10^{-8}

2.2. One-dimensional oedometer tests

The R-B mixes were subjected to one-dimensional oedometer swelling and shrinkage tests. For this, the different R-B mixes were pre-wetted with distilled water (DW) to reach their corresponding optimum moisture content (OMC). Identical R-B specimens were then prepared by compacting the required amount of these soil mixes into oedometer rings with a diameter of 75 mm and a height of 30 mm, compacted to a height of 20 mm. The oedometer rings were then placed between two Whatman No. 1 filter papers and two dry porous stones and the assemblies were transferred into the oedometer swell setups. The dial gauges were affixed and the load corresponding to 12.5 kPa was placed on the soil specimens. Then the specimens were inundated with either DW or 0.4 M NaCl or $CaCl_2$ solution. The specimens were left undisturbed till the secondary swell was completed and the dial gauge readings were also noted down to measure the percentage swell with time. At the end of swelling cycle, the fluid from the oedometer jackets was drained and the specimens with the vertical load were placed in an oven under a controlled temperature of 45 ± 2 °C to accelerate the drying process. This temperature also simulates the average landfill operating temperature, which ranges between 30 and 60 °C (Mallick et al., 2024). The specimens were dried completely after drying for about five to six days in the oven. Complete drying was confirmed by the stabilization of their weight, indicating no further reduction in weight and water content. After complete

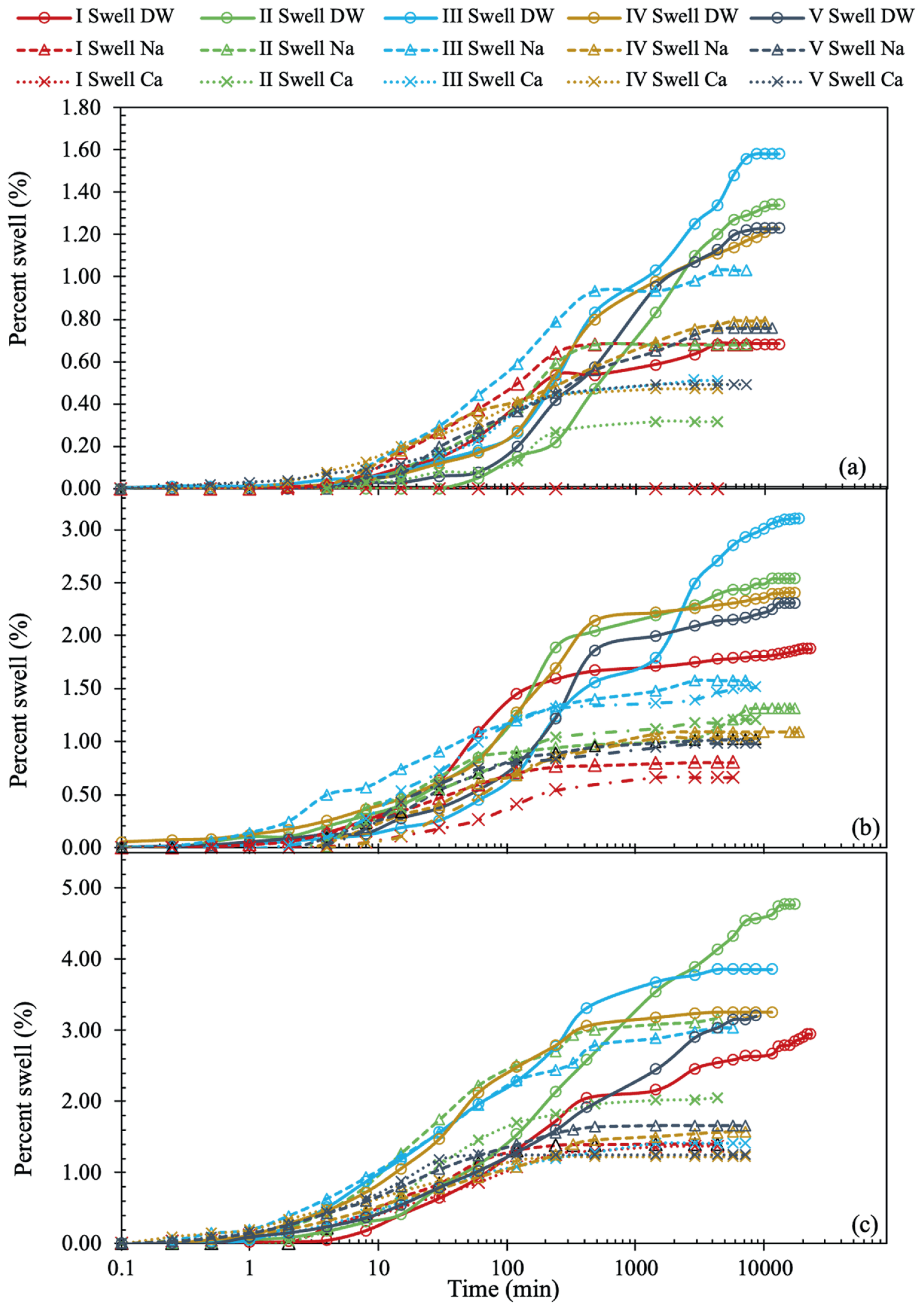

Fig. 2. Comparison of time-swell plots of red soil-bentonite mixtures: (a) 90R-10B, (b) 80R-20B and (c) 70R-30B specimens during wetting cycles using different inundating fluids.

drying of the specimens, the specimens were again transferred to the swell test setups and inundated with the same inundating fluid as used previously, and the process was repeated for five wet-dry cycles until the vertical deformations achieved equilibrium.

2.3. Microstructure analyses

The microstructure of the compacted R-B mixes was examined using the SEM and MIP on soil specimens collected after selected cycles of wetting and drying. Duplicate tests were conducted for both SEM and MIP to ensure the reliability of the results obtained. The tests were done on small portions of compacted specimens extruded from the whole specimens using a sampler of inner diameter 10 mm and height of 30 mm. Undisturbed wet soil samples were obtained by carefully pushing the sampler tube into the specimens. To preserve the soil structure, the samples were frozen for at least 24 h, followed by lyophilisation under deep vacuum conditions. For SEM analysis, the samples were mounted on aluminium discs and gold-coated under high vacuum using a sputtering machine prior to imaging. The tests were carried out using a high-resolution scanning electron microscope (Quanta 200). The MIP tests were carried out in a Thermo Scientific – Pascal Mercury Porosimeters (140, 440 series) device.

Image analysis was performed using the ImageJ Fiji software on digital camera images of the compacted soil surfaces after different wetting cycles. This analysis supplemented the MIP test results, as the MIP equipment cannot detect the large pores (>135 μm) (Devapriya and Thyagaraj, 2024). After scaling the images, a 4 cm^2 representative area was selected for the analysis. The selected area was then converted to binary images using suitable threshold values ranging from 73 to 100 (Devapriya and Thyagaraj, 2024). Pores with diameter greater than 135 μm were identified and counted using the ImageJ Fiji software and their areas were calculated.

2.4. Hydraulic conductivity tests

The hydraulic conductivity tests were conducted on identical compacted soil specimens after the completion of swelling following each wetting cycle using rigid-wall and flexible-wall permeameters. The tests were carried out using the same permeating fluid that was used for inundation during the oedometric swelling. The rigid-wall tests were carried out using the variable head method in accordance with the ASTM D5856-15 (2015) under a surcharge pressure of 12.5 kPa and hydraulic gradient of 20.

While the rigid wall permeability tests give quick results, they cannot simulate various overburden pressures expected at field conditions. Therefore, the hydraulic conductivity tests were also conducted using flexible wall permeability tests at different effective confining pressures of 20 kPa, 50 kPa and 100 kPa that is expected to simulate different waste heights at various stages of landfilling (Ramesh and Thyagaraj, 2022). The flexible-wall tests were conducted using the constant head method in accordance with the ASTM D5084-16 (2016) under a pressure head of 5 kPa, which corresponds to a hydraulic gradient of 20–25, depending on the height of the swollen specimens.

The flexible-wall testing was conducted in three distinct phases: saturation, consolidation and permeation. During the saturation phase, the soil specimens were back pressurized at 140 kPa, 190 kPa and 240 kPa and 290 kPa under the corresponding cell pressures of 150 kPa, 200 kPa, 250 kPa and 300 kPa, respectively. At each stage, the permeating fluid was allowed to flow through the specimen from the inflow tube to the outflow tube. The specimens were considered fully saturated at a particular pressure stage when inflow and outflow rates were equal, after which the pressure was increased to the next stage. Following saturation, the soil specimens were consolidated at a confining pressure of 20 kPa, following which the hydraulic conductivity was measured under a constant pressure gradient of 5 kPa. The tests were terminated upon achieving the steady-state advective flow, based on stable hydraulic conductivity, inflow/outflow ratio of 0.75–1.25, and

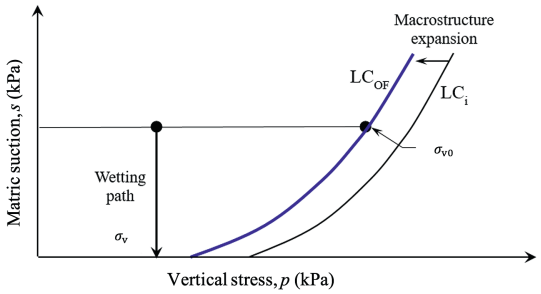

Fig. 3. Schematic diagram showing the shifting of LC curves in specimens subjected to wetting using salt solution.

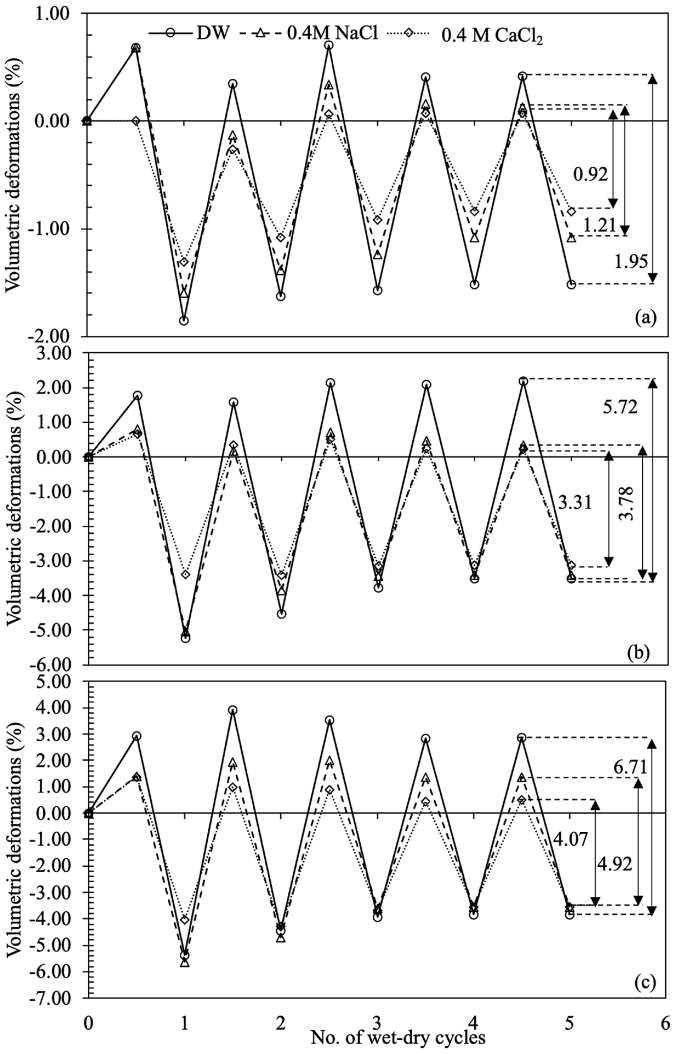

Fig. 4. Variation of volumetric deformations of (a) 90R-10B, (b) 80R-20B and (c) 70R-30B specimens subjected to wet-dry cycles using DW, 0.4M NaCl and 0.4M $CaCl_2$ solutions.

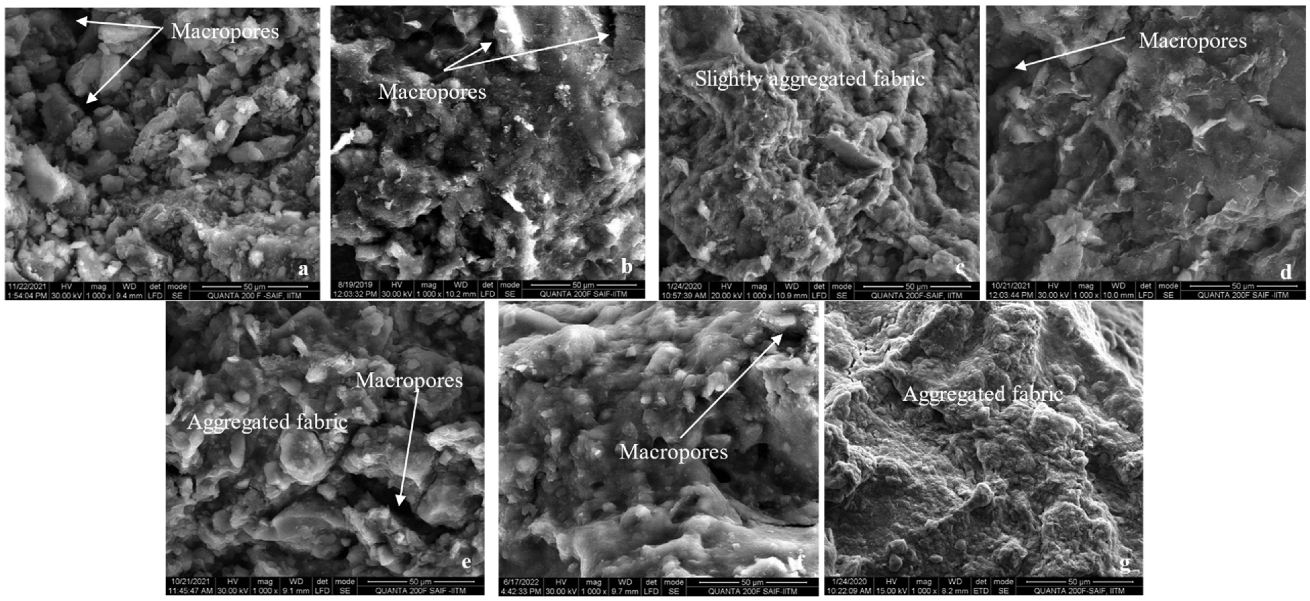

Fig. 5. SEM micrographs of 90R-10B specimen: (a) in as-compacted state, (b) after 1st wetting with DW, (c) after 5th wetting with DW, (d) after 1st wetting with NaCl solution, (e) after 5th wetting with NaCl solution, (f) after 1st wetting with $CaCl_2$ solution, and (g) after 5th wetting with $CaCl_2$ solution.

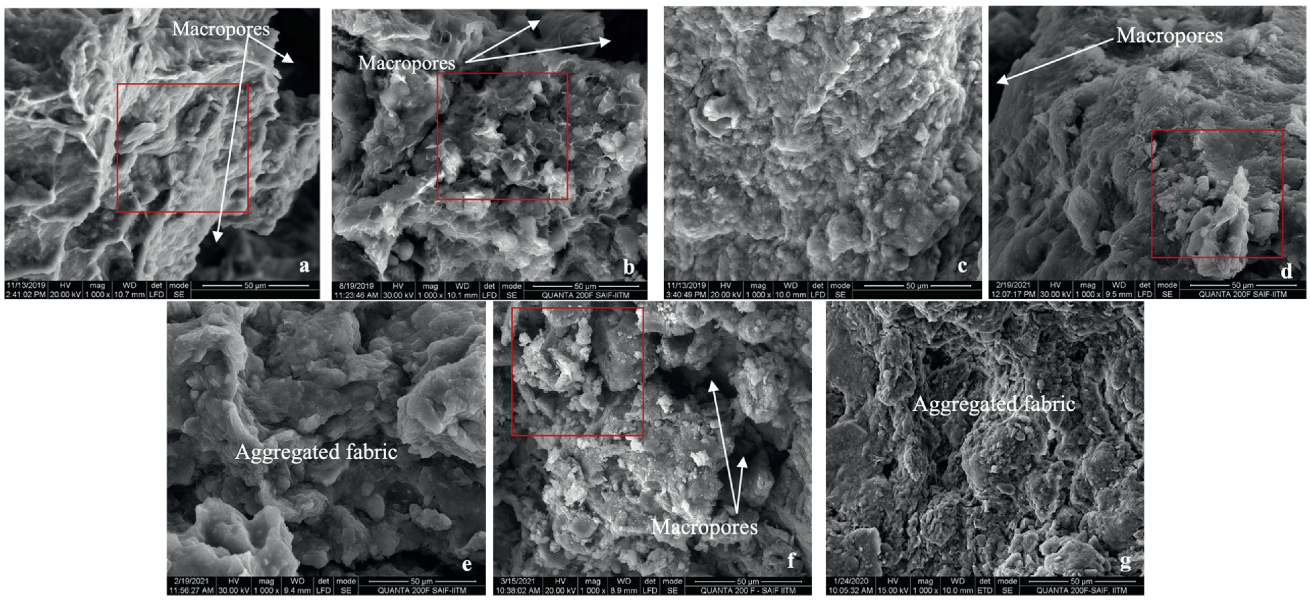

Fig. 6. SEM micrographs of 80R-20B specimen: (a) in as-compacted state, (b) after 1st wetting with DW, (c) after 5th wetting with DW, (d) after 1st wetting with NaCl solution, (e) after 5th wetting with NaCl solution, (f) after 1st wetting with $CaCl_2$ solution, and (g) after 5th wetting with $CaCl_2$ solution.

passage of at least 2 pore volumes, in accordance with ASTM D7100-11, (2020). Monitoring of chemical equilibrium was not performed, as the study considered only the advective flow and did not address the diffusive or chemical transport processes. The confining pressure was later increased to 50 kPa and 100 kPa, and the hydraulic conductivity was measured after each stage of consolidation.

3. Results and discussion

3.1. Combined effect of chemical contamination and wet-dry cycles on volume change behaviour

As mentioned in the previous section, the R-B mixes were subjected to five alternate wet-dry cycles using three inundating fluids: DW, 0.4 M NaCl solution and 0.4 M $CaCl_2$ solution. The time-swell plots of R-B mixes permeated with DW, 0.4 M NaCl and 0.4 M $CaCl_2$ solutions during different wetting cycles are differentiated in Fig. 2. These time-swell plots can be demarcated into three zones: (i) the initial flat portion called the initial swell phase, (ii) the rapidly rising primary swell phase and (iii) the final plateau called the secondary swell phase. The S-shaped trend is prevalent in all the specimens except in the 90R-10B specimen inundated with $CaCl_2$ solution during 1st wetting cycle, where no measurable vertical swell was observed.

It is clear that the amount of bentonite and the type of cation in the inundating fluid affect the initiation and progression of the primary swelling in the R-B specimens. The percent swell as well

as the primary swell is maximum in specimens inundated with DW, and least in specimens inundated with 0.4 M $CaCl_2$ solution. The onset of initial and primary swell is also quicker with the increase in the bentonite content.

For the 90R-10B specimen, the absence of vertical swelling during the first wetting cycle using $CaCl_2$ solution is attributed to the combined effects of low bentonite content and strong osmotic suction induced by divalent cations, which restricted particle expansion to inter-void swelling alone. However, in subsequent wetting cycles, vertical deformation became evident. The increased matric suctions in completely dried 90R-10B specimen resulted in the increased swell potential during the subsequent wetting cycles, leading to a delayed yet observable primary swell phase in later cycles. In contrast, specimens with higher bentonite content (80R-20B and 70R-30B) exhibited immediate vertical swelling even in the presence of $CaCl_2$ solution, with a well-defined primary swell phase. Their swell magnitudes were consistently higher, and the time to reach primary swell was shorter compared to lower bentonite content specimens. The suppressive effect of Na^+ ions was less significant than that of Ca^{2+} ions, allowing moderate swell development in 0.4 M NaCl solution.

The compacted soil specimens in their as-compacted state are unsaturated and are characterised by the matric suction. Dissipation of the matric suction on inundation with fluids results in the swelling of the specimens (Rao and Thyagaraj, 2007). The presence of salt solutions modifies this response through osmotic interactions, further influencing the swelling potential. When the soil specimens are inundated with salt solutions, the osmotic gradient induced between the reservoir fluid and the pore fluid is dissipated by the inward salt diffusion and osmotic outward flow from the soil pore water (Rao and Thyagaraj, 2007). The inward diffusion of the salts into the soil pore space reduces the DDL thickness, which in turn decreases the swell potential of the compacted soil specimens (Rao et al., 2006; Castellanos et al., 2008; Thyagaraj and Rao, 2015; Thyagaraj et al., 2016). The osmotic induced consolidation also plays a role in reducing the swell potential. However, the magnitude of osmotic induced consolidation is based on the osmotic efficiency of clay soils. The magnitude of osmotic induced consolidation is negligible in comparison to the osmotic consolidation. The micropores volume decreases on account of the increase in the concentration of pore fluid, and tends to increase in the macropores volume, resulting in the macrostructural expansion (i.e., chemical softening) during wetting (depicted through microstructure in section 2.2). This can be regarded as equal to the leftward movement of the Loading-Collapse (LC) curve in the $\sigma_v - s$ space, as represented schematically in Fig. 3 (Gens and Alonso, 1992; Sanchez et al., 2005; Thyagaraj and Das, 2017). As the LC curve shifts leftward from LC_i to LC_{OF}, the distance between the applied stress state (σ_v) and the yield stress σ_{v0} reduces, leading to an increase in the ratio of σ_v/σ_{v0}. Hence, the swelling strain recorded in the compacted R-B specimens reduces with the increase in concentration of the inundating fluids.

Fig. 4 illustrates the changes in volumetric deformations with wet-dry cycles of R-B specimens wetted with DW and inorganic salt solutions. For all the inundating fluids used, the specimens are seen to reach equilibrium volumetric deformation by the 5th cycle, where the swell-shrink paths become reversible. Fig. 4 shows that in addition to the reduction in the swell, the physico-chemical changes brought out by the salt solutions also reduce the shrinkage of the R-B specimens. The increase in the salt concentration in the soil pore fluid, as the matric and osmotic suctions dissipate during the swelling cycle, alters the chemistry of the soil pore fluid. The increased concentration of Na^+ or Ca^{2+} ions decreases the DDL thickness, which effectively reduces the net particle repulsion between the soil aggregates (Rao et al., 2006; Chen et al., 2022). This results in increased aggregation of the soil particles. The SEM images and EDAX analysis presented in Figs. 5–8 (and discussed in detail in section 2.2) support this discussion. The decreased swell-shrink potentials with increased induced osmotic gradient result in the equilibrium bandwidths of the specimens following the order: DW > 0.4 M NaCl solution >0.4 M $CaCl_2$ solution.

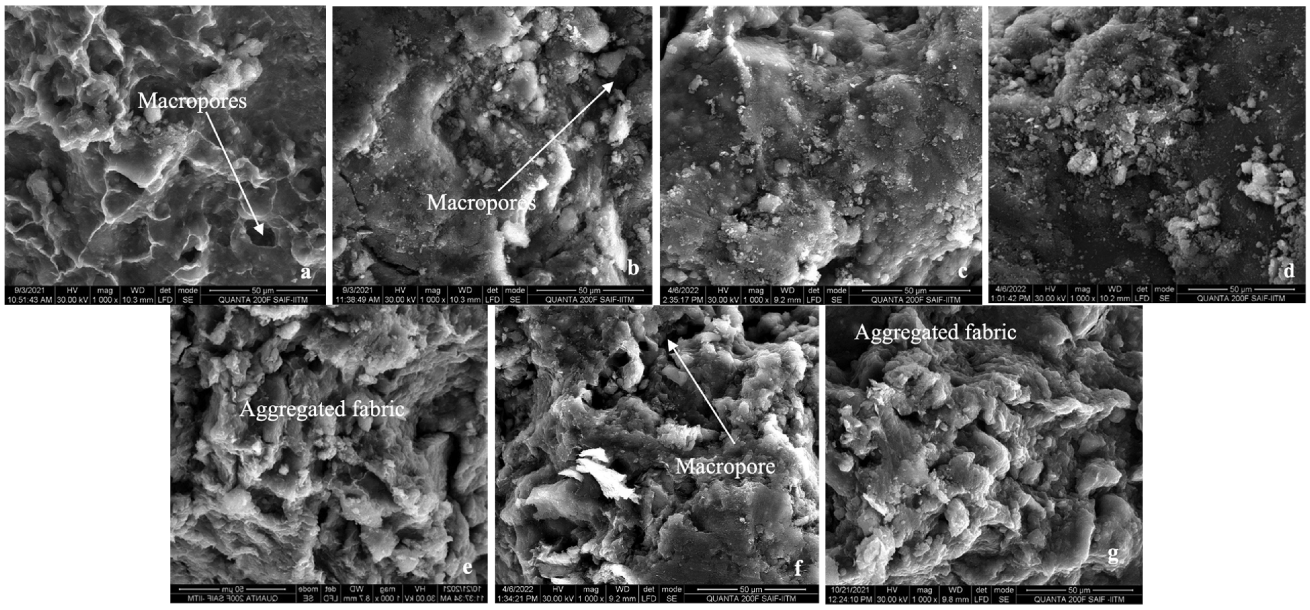

Fig. 7. SEM micrographs of 70R-30B specimen: (a) in as-compacted state, (b) after 1st wetting with DW, (c) after 5th wetting with DW, (d) after 1st wetting with NaCl solution, (e) after 5th wetting with NaCl solution, (f) after 1st wetting with $CaCl_2$ solution, and (g) after 5th wetting with $CaCl_2$ solution.

3.2. Microstructure changes in R-B specimens subjected to wet-dry cycles and chemical contamination

Figs. 5–7 present the SEM micrographs of 90R-10B, 80R-20B and 70R-30B specimens in the as-compacted state and following 1st and 5th (equilibrium) wetting cycles when inundated with DW, 0.4 M NaCl and 0.4 M $CaCl_2$ solutions. The SEM micrograph captures the double structure of the compacted R-B specimen in its as-compacted state. On subjecting the compacted soil specimens to first wetting, irrespective of the inundating fluid, the micropores expand in volume, leading to the reduction of macropore size in the soil specimens. Even in the swollen state, the specimens retain the double structure with both the macropores and the micropores in the soil fabric. EDAX evaluation conducted on the 80R-20B specimen (Fig. 8) indicates an increase in the elemental weight of Na^+ and Ca^{2+} ions on the soil fabric when inundated with 0.4 M NaCl and 0.4 M $CaCl_2$ solutions, respectively. The SEM micrographs of specimens that underwent wet-dry cycles using salt solutions show more particle aggregation than the specimens wetted with DW, which can be ascribed to the decrease in the repulsive forces in the soil fabric, due to the increase in concentration of salt solutions. Particle aggregation is visibly more for soils inundated with $CaCl_2$ solution than with NaCl solution, due to the higher valency of the Ca^{2+} ions, which results in stronger electrostatic attraction between the soil particles. Similar results were presented by Thyagaraj and Salini (2015), Manca et al. (2016) and Lin et al. (2022). The soil fabric of specimens inundated with salt solutions also appears comparatively rougher than the DW inundated specimens due to suppression of DDLs, which is consistent with the findings of Zou et al. (2018).

The results of the MIP tests carried out on R-B specimens complement and enhance the SEM analysis. Figs. 9–11 and Fig. 14a–b, 15a-b and 16a-b show the PSD functions and cumulative intruded mercury void ratio (e_{Hg}) plots obtained from the MIP

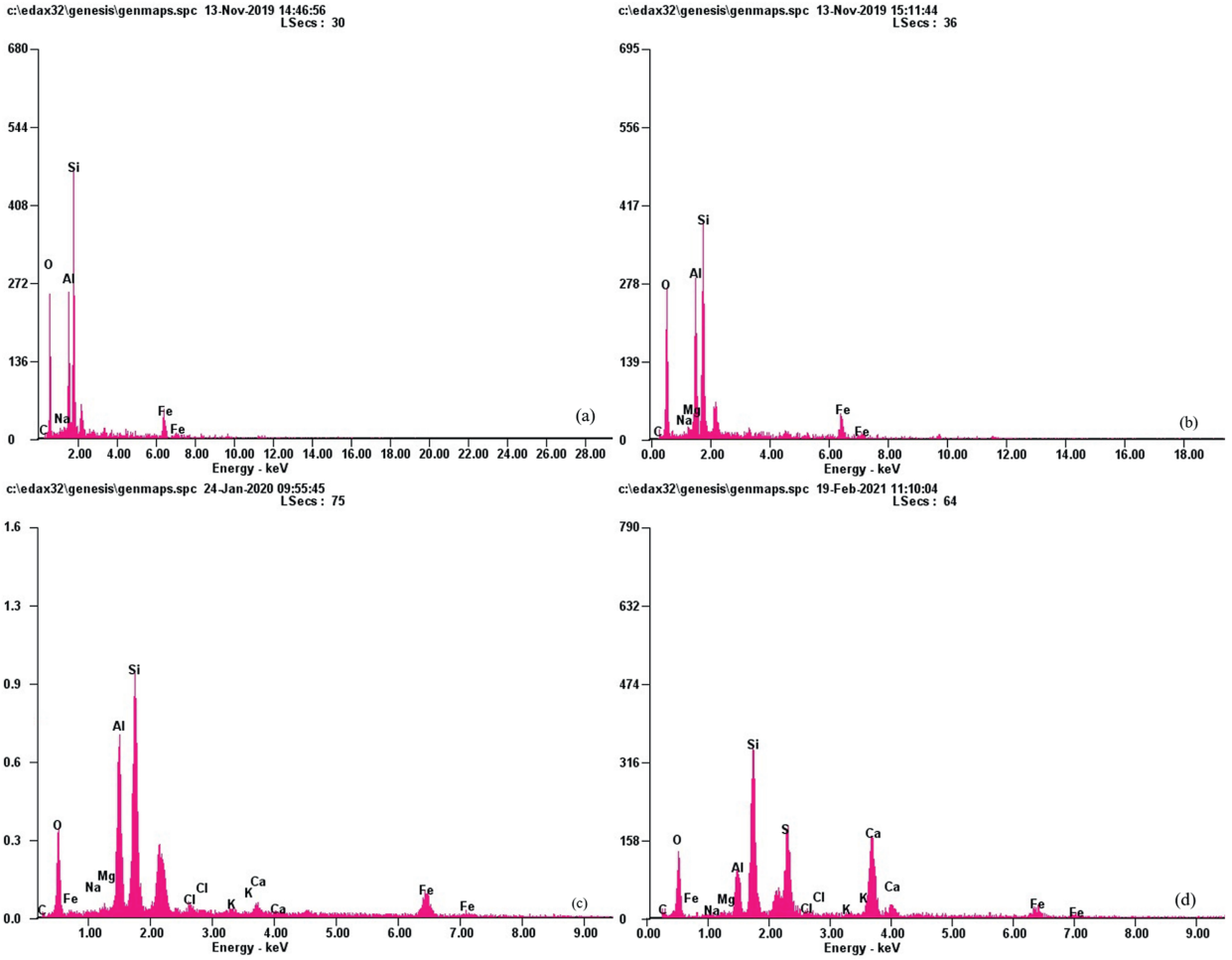

Specimen	IF	Cycle	EDAX Fig. No.	SEM Fig. No.	Elemental weight (%)									
					Al	Si	Fe	C	O	Mg	K	Na	Ca	Cl
R80-B20	-	AC	a	6a	15.09	28.96	12.45	5.00	37.83	-	-	0.66	-	-
	DW	1st wet	b	6b	13.55	26.10	17.61	9.57	31.5	-	-	0.53	-	-
	NaCl		c	6c	16.47	30.74	11.19	7.14	29.43	1.09	0.94	2.35	-	0.64
	$CaCl_2$		d	6d	5.37	16.87	2.71	17.04	37.92	0.35	0.36	0.58	8.83	0.39

Fig. 8. EDAX elemental analysis of 80R-20B specimen: (a) in as-compacted state and after 5th swell when inundated with (b) DW, (c) NaCl and (d) $CaCl_2$ solutions.

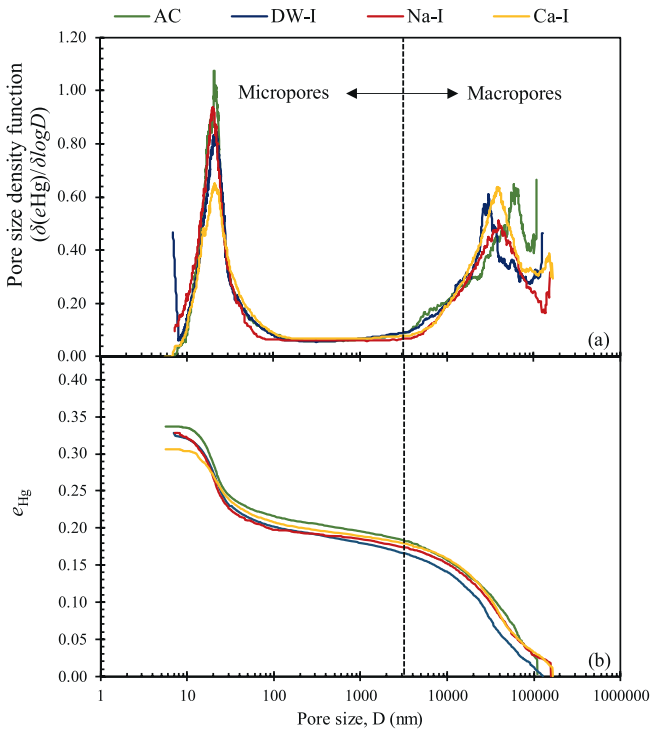

Fig. 9. Comparison of (a) PSD and (b) e_{Hg} of 90R-10B specimen in its as-compacted state and after first wetting using DW, 0.4M NaCl and 0.4M $CaCl_2$ solutions.

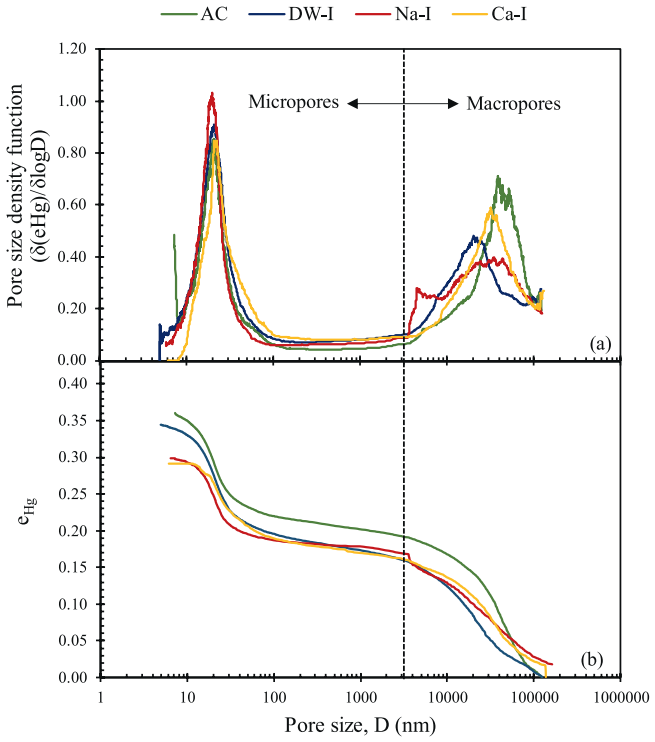

Fig. 10. Comparison of (a) PSD and (b) e_{Hg} of 80R-20B specimen in its as-compacted state and after first wetting using DW, 0.4M NaCl and 0.4M $CaCl_2$ solutions.

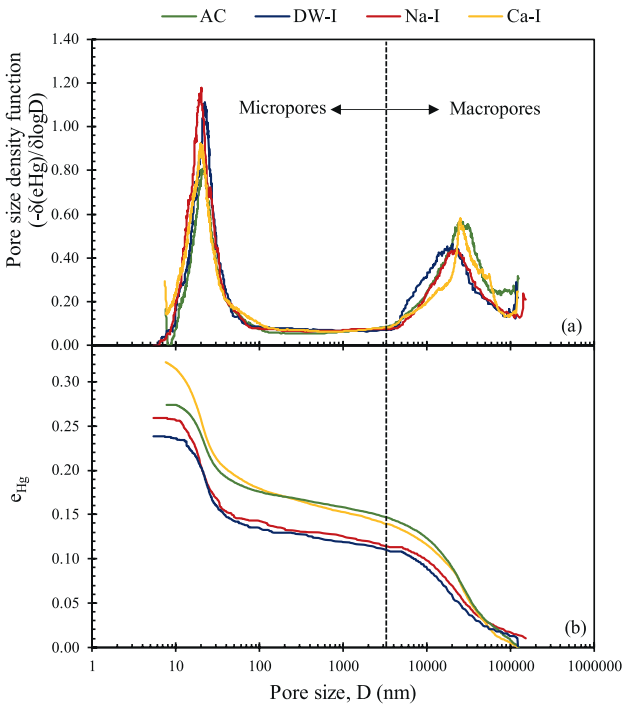

Fig. 11. Comparison of (a) PSD and (b) e_{Hg} of 70R-30B specimen in its as-compacted state and after first wetting using DW, 0.4M NaCl and 0.4M $CaCl_2$ solutions.

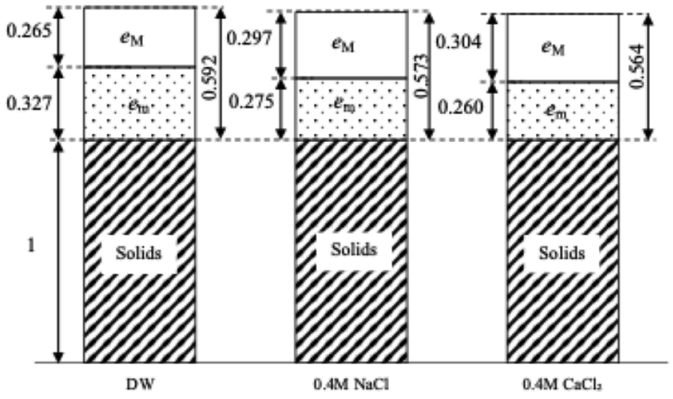

Fig. 12. Phase diagram of 80R-20B specimen after 1st wetting cycle when inundated with DW, 0.4M NaCl and 0.4M $CaCl_2$ solutions.

studies on 90R-10B, 80R-20B and 70R-30B specimens, respectively. The PSD distributions of all three compacted R-B specimens with varying bentonite contents exhibit a distinct bimodal pattern, irrespective of the inundating fluid used during the wetting cycles, which is consistent with the double structure observed in the SEM micrographs. The two modes of the PSDs show the existence of pore volumes in two dominant size ranges: the macropore volume which is the inter-aggregate pore volume corresponding to the pores between the red soil and bentonite aggregates; and the micropore volume, which is the intra-aggregate pore volume corresponding to the pores within the bentonite aggregate. The delimiting size of the macropore volume is considered as 4 μm,

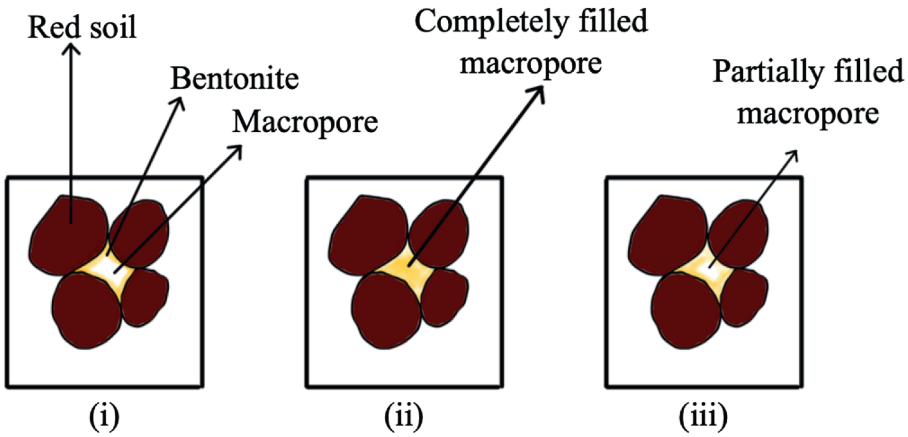

Fig. 13. Schematic diagram of bentonite filling the macropores in the compacted R-B mixes in (a) as-compacted state, (b) specimen inundated with DW and (c) specimen inundated with salt solutions.

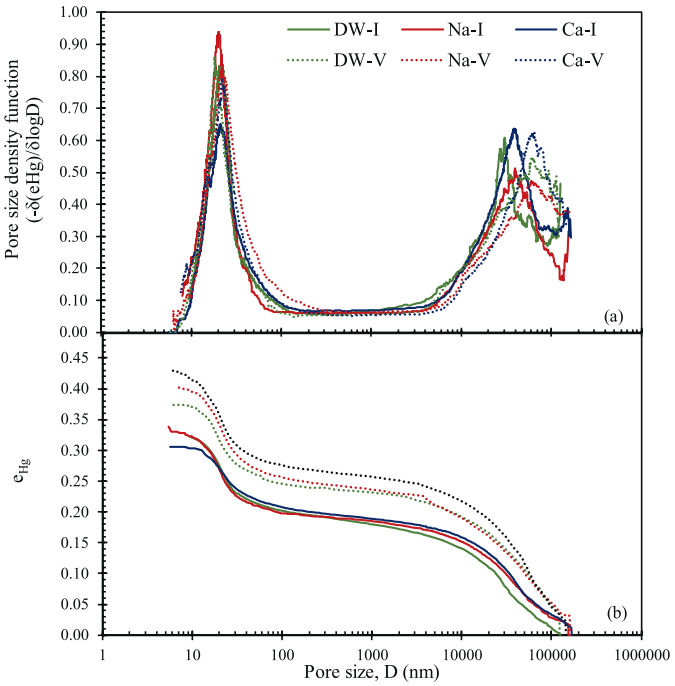

Fig. 14. Comparison of change in the (a) PSD and (b) e_{Hg} of 90R-10B specimen during first and equilibrium wetting cycle using DW, 0.4M NaCl solution and 0.4M $CaCl_2$ solution.

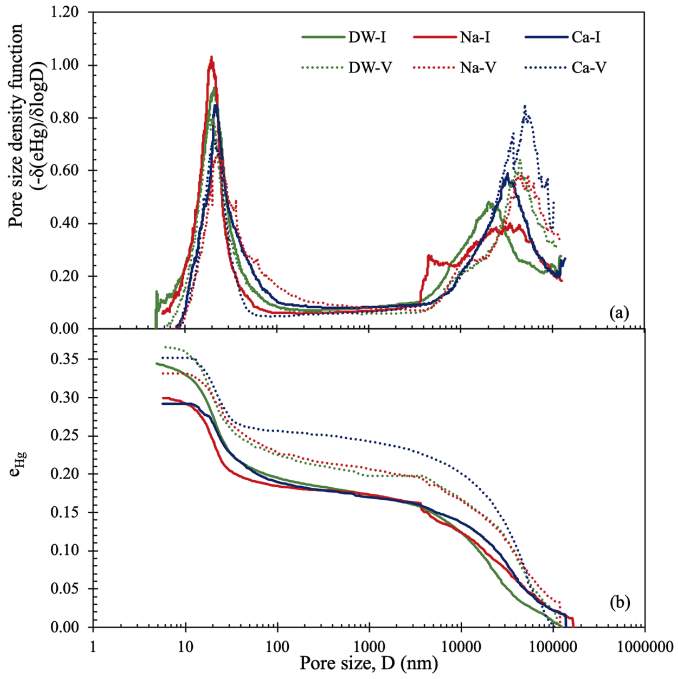

Fig. 15. Comparison of change in the (a) PSD and (b) e_{Hg} of 80R-20B specimen during first and equilibrium wetting cycle using DW, 0.4M NaCl solution and 0.4M $CaCl_2$ solution.

where the base of the macropore mode starts, in all the R-B specimens.

Fig. 9a–b, 10a-b and 11a-b show the effect of the type of inundating fluid during the first wetting cycle on the PSD and e_{Hg} of compacted 90R-10B, 80R-20B and 70R-30B specimens. The figures show that on subjecting the specimens to wetting, the macropores peak modes of the swollen specimens shift leftward of the as-compacted macropores peak mode, irrespective of the inundating fluid. This shift in the macropores mode is attributed to the DDL expansion in response to the matric suction dissipation in the specimens, which results in the increased micropores volume, which in turn reduces the macropores volume in the specimens. It can also be noted that even though the 90R-10B specimen inundated with 0.4 M $CaCl_2$ solution shows zero vertical deformation (Figs. 2 and 4) during the 1st wetting cycle, the macropores mode of the specimen shows a leftward shift, confirming that the inter-voids swelling has taken place in the specimen.

Further observation of the MIP results in Figs. 9–11 show that the macropores peak mode of the R-B specimens inundated with different fluids follows the order of DW < 0.4 M NaCl solution <0.4 M $CaCl_2$ solution. This follows the same order as that of the swell potential exhibited with the soil specimens. The osmotic and induced osmotic consolidation result in the decrease of the micropores, resulting in increased macropores in the soil specimen. Fig. 12 depicts the same in the phase diagrams for 80R-20B specimens after the 1st wetting cycle when inundated with DW, 0.4 M

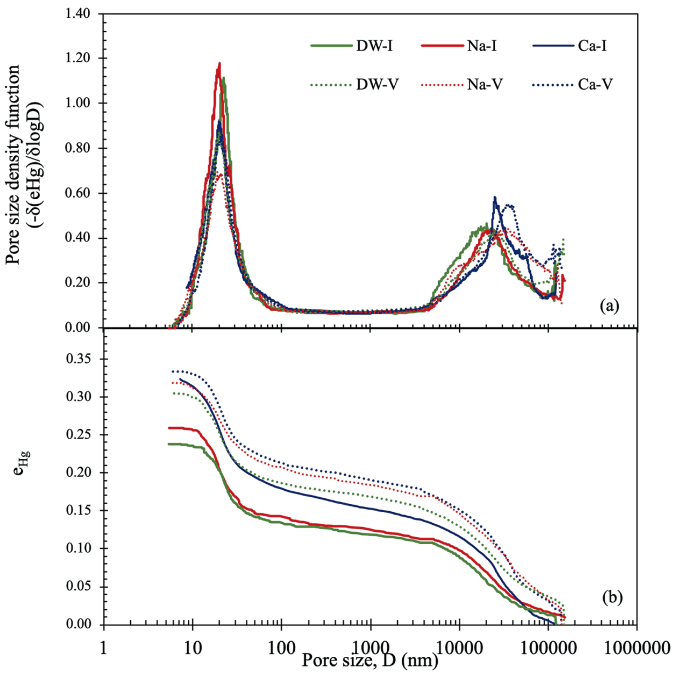

Fig. 16. Comparison of change in the (a) PSD and (b) e_{Hg} of 70R-30B specimen during first and equilibrium wetting cycle using DW, 0.4M NaCl solution and 0.4M $CaCl_2$ solution.

NaCl, 0.4 M $CaCl_2$ solutions during the 1st wetting cycle. The void ratio in the specimens is comprised of: macropores voids (e_M) and micropores voids (e_m). Since the MIP equipment results in undetected pores, e_M is considered to be equal to the cumulative intruded pore volume at 4 μm scaled to $\left(e_{lim}/e_{Hg_{max}}\right) \times e$, where e_{lim} is the cumulative mercury intruded void ratio at delimiting macropore size (4 μm), $e_{Hg_{max}}$ is the maximum cumulative mercury intruded void ratio obtained using MIP and e is the global void ratio of the specimen. e_m is considered as equal to the difference between e and e_M.The figure shows that as the induced osmotic suction of the inundating fluids increases, the global void ratio of the specimens and the micropores void decreases, but the macropores voids in the soil specimens increases. This results in macrostructural softening in the soil specimens. As the macropores in the soil specimens increase, the leftward shift of the macropores mode reduces, and the diameter of the macropores peak is the highest in specimens inundated with $CaCl_2$ solution. A similar decrease in the reduction of the macropores with increased induced osmotic suction due to increased concentration of the inundating fluids was observed by Manca et al. (2016) and Thyagaraj and Julina (2019). The macropores peak modes also increase with the decrease in bentonite content and the resulting decrease in the overall DDL thickness. Observation of the e_{Hg} plots show that the cumulative intruded mercury void ratio is also more in the specimens inundated with salt solution when compared to the e_{Hg} of the DW-inundated specimens. This is also in response to the increased micropores expansion of the bentonite in the DW

Images	90R-10B specimen			
	AC	I Wetting DW	I Wetting 0.4M NaCl	I wetting 0.4M $CaCl_2$
Total area	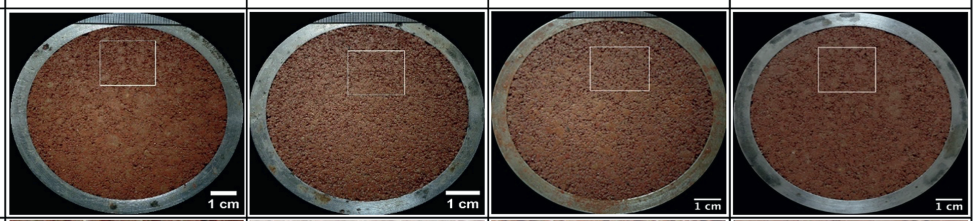			
Selected area (4cm²)	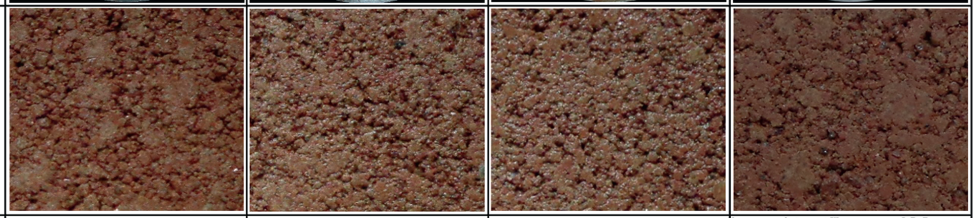			
Binary image of the selected area	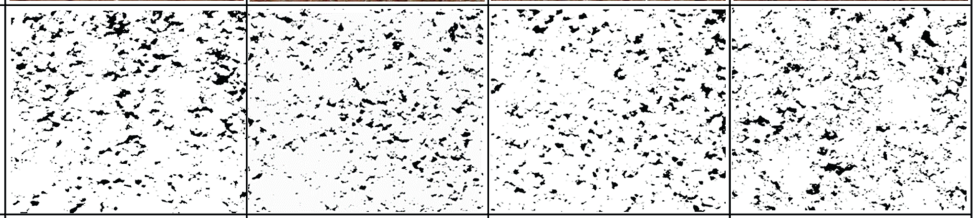			
Area of macropores (cm²)	0.424	0.33	0.367	0.417
Area of macropores of dia>135 μm (cm²)	0.402	0.30	0.345	0.379

Fig. 17. Digital camera images, selected area and the corresponding binary images of 90R-10B specimen in its as-compacted state and after 1st wetting cycle using various inundating fluids.

Images	90R-10B specimen		
	II Wetting DW	II Wetting 0.4M NaCl	II wetting 0.4M $CaCl_2$
Total area	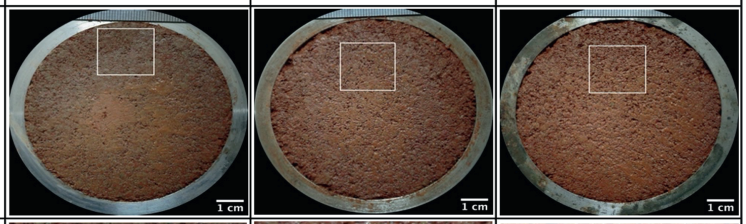		
Selected area (4cm²)	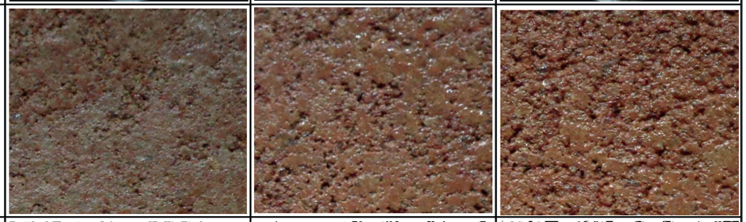		
Binary image of the selected area	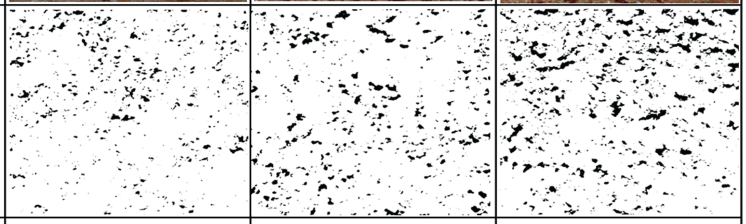		
Area of macropores (cm²)	0.166	0.253	0.387
Area of macropores of dia>135 μm (cm²)	0.144	0.233	0.359

Fig. 18. Digital camera images, selected area and the corresponding binary images of 90R-10B specimen after 2nd wetting cycle using various inundating fluids.

inundated specimens which result in larger closing of the macropores. The kaolinite mineral in the red soil remains mostly inert, whereas the bentonite undergoes volume change (Devapriya and Thyagaraj, 2024) (Fig. 13).

Figs. 14–16 (a, b) demonstrate the combined effect of type of inundating fluid and wet-dry cycles on the PSD and e_{Hg} plots of the 90R-10B, 80R-20B and 70R-30B specimens, respectively. In addition to the increase in the macropores size with the induced osmotic suction, the wet-dry cycles also alter the PSDs in soil specimens. The macropores mode is larger in the soil specimens at the end of the 5th wetting cycle, as compared to the 1st wetting cycle. The e_{Hg} plots of the specimens after the 5th cycle also lie above the e_{Hg} plots of the specimens after the 1st cycle. The macropores peak diameter and e_{Hg} is the highest in specimens inundated with 0.4 M $CaCl_2$ solution because of the higher charge of the Ca^{2+} cations.

The alternate wet-dry cycles result in continuous rearrangement of the soil particles, which alter the PSD of the compacted soil specimens. Devapriya and Thyagaraj (2024) showed that when the compacted R-B specimens were subjected to wet-dry cycles using DW, the redistribution of the PSD resulted in more macropores of size <135 μm, which were initially of sizes >135 μm. Since the MIP equipment cannot capture larger macropores (>135 μm), the detected macropores were lesser during the initial cycles, but increases at the end of the equilibrium cycle, resulting in a slight rightward movement in the macropores peak in DW inundated specimens.

Digital camera image analysis was carried out to supplement the MIP tests on specimens inundated with distilled water and salt solutions. Figs. 17–20 present the digital camera images of total area, representative area (4 cm^2) along with the respective binary images of 90R-10B specimen after 1st, 2nd, 3rd and equilibrium wetting cycles using various inundating fluids. The calculated area of macropores obtained through the image analysis also shows that while the macropores reduce during the initial cycles of wetting, by the end of the 5th wetting cycle, the macropores in the specimen increases when inundated with salt solutions, thus corroborating with the MIP results. The observations made through the SEM analysis are also consistent to this result. The digital camera image analysis also shows the increased macropores with increased induced osmotic suction. Thus, the chemical contamination along with the wet-dry cycles is seen having a higher impact than the wet-dry cycles using DW on the PSD of the compacted R-B specimens.

Images	90R-10B specimen		
	III Wetting DW	III Wetting 0.4M NaCl	III wetting 0.4M $CaCl_2$
Total area	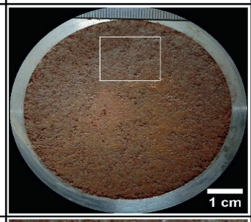	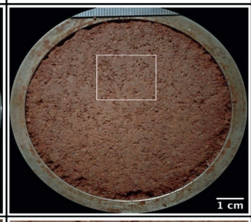	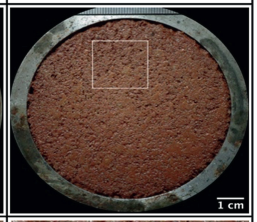
Selected area ($4cm^2$)	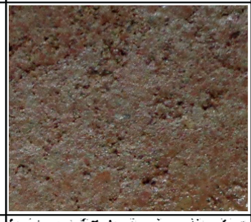	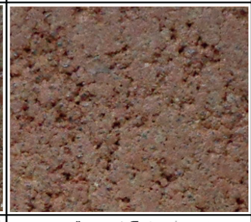	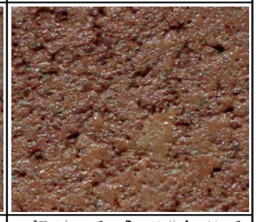
Binary image of the selected area	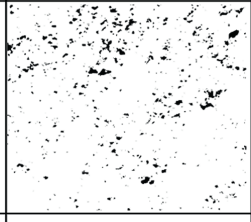	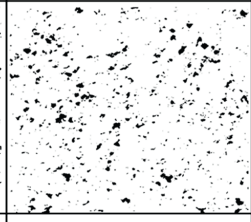	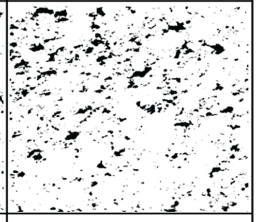
Area of macropores (cm^2)	0.151	0.209	0.353
Area of macropores of dia>135 μm (cm^2)	0.128	0.181	0.321

Fig. 19. Digital camera images, selected area and the corresponding binary images of 90R-10B specimen after 3rd wetting cycle using various inundating fluids.

3.3. Hydraulic performance of compacted R-B mixes subjected to wet-dry cycles and chemical contamination

Fig. 21 illustrates the effect of bentonite content and type of inundating fluids on the hydraulic conductivity of the compacted R-B mixes measured using the rigid wall apparatus. The hydraulic conductivity of the specimens follows the order: DW inundated specimens <0.4 M NaCl solution inundated specimens <0.4 M $CaCl_2$ solution inundated specimens. This is attributed to the lower swelling ability of the specimens with the induced osmotic suction that reduces the bound water in the soil specimen owing to the suppression of the DDLs which results in higher macropores in the specimens.

Figs. 22,23 and 24a-c illustrate the combined effect of wet-dry cycles and chemical contamination on the hydraulic behaviour of compacted 90R-10B, 80R-20B and 70R-30B specimens, at cell pressures of 20 kPa, 50 kPa and 100 kPa, respectively. The hydraulic conductivity shows an overall increasing trend with the wet-dry cycles, irrespective of the inundating fluids. However, the salt solutions have a more detrimental effect on the hydraulic conductivity of the specimens, with specimens showing very high hydraulic conductivity by the end of the equilibrium cycle. The higher hydraulic conductivity in salt solutions inundated specimens is due to the formation of interconnected network of pores due to extensive aggregation of particles as explained in the previous section.

The hydraulic behaviour of the compacted R-B mixes during wet-dry cycles is governed by the bentonite content and concentration and cation valency of the inundating fluids. 90R-10B specimen exhibited higher hydraulic conductivity than the design recommendation of 1×10^{-7} cm/s after 3 cycles of wetting and drying when inundated with DW, and the same specimen exhibited much larger hydraulic conductivity when inundated with salt solutions, right from the first cycle of wetting (Fig. 22). Further, the 90R-10B specimen inundated with 0.4 M NaCl solution satisfied the hydraulic conductivity design criteria only during the 1st cycle of wetting, while it required higher cell pressure of 100 kPa to meet the design requirement upon inundation with 0.4 M $CaCl_2$ solution. Both 80R-20B and 70R-30B specimens subjected to wet-dry cycles using DW satisfy the hydraulic conductivity criterion even after 5 cycles of wetting and drying (Figs. 23 and 24). 80R-20B specimen conforms to the hydraulic conductivity criterion when saturated with the salt solutions during the 1st wetting cycle, even at lower confining pressure. At the confining pressure of 100 kPa, 80R-20B specimen inundated with 0.4 M NaCl solution satisfied the hydraulic conductivity criterion up to 3

Images	90R-10B specimen		
	V Wetting DW	V Wetting 0.4M NaCl	V wetting 0.4M $CaCl_2$
Total area	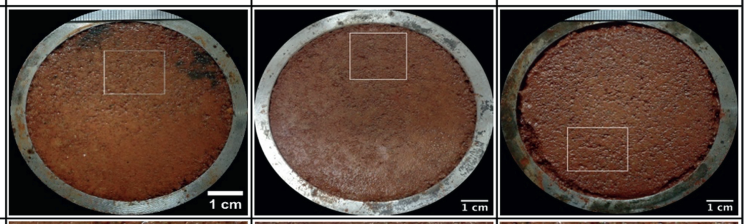		
Selected area ($4cm^2$)			
Binary image of the selected area	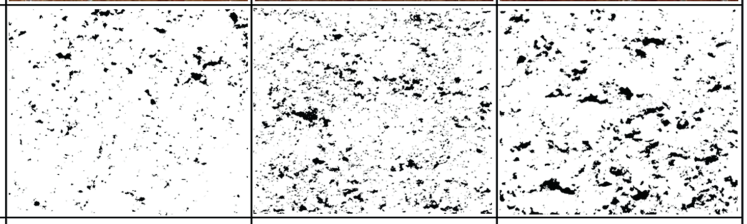		
Area of macropores (cm^2)	0.147	0.301	0.400
Area of macropores of dia>135 μm (cm^2)	0.127	0.364	0.428

Fig. 20. Digital camera images, selected area and the corresponding binary images of 90R-10B after 5th wetting cycle using various inundating fluids.

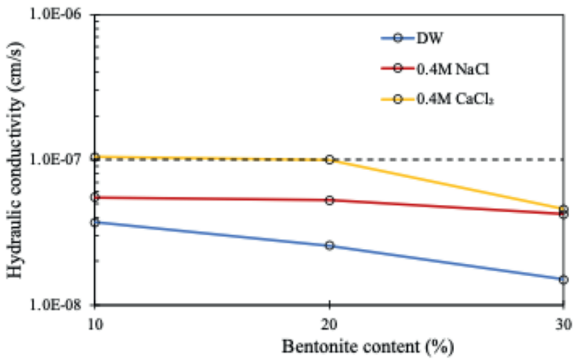

Fig. 21. Effect of bentonite content and type of inundating fluid on hydraulic conductivity of compacted R-B mixes.

cycles, beyond which the value was above the design criterion. However, even the higher confining pressure of 100 kPa was not sufficient to bring down the hydraulic conductivity values when inundated with 0.4 M $CaCl_2$ solution (Fig. 23). Finally, 70R-30B specimen meets the hydraulic conductivity criterion at the end of equilibrium wet-dry cycle using DW and 0.4 M NaCl solution, even at lower confining pressures. However, a higher confining pressure of 100 kPa was required to meet the hydraulic conductivity criterion when inundated with 0.4 M $CaCl_2$ solution (Fig. 24).

To understand the relation between hydraulic conductivity and pore structure variation under chemical contamination and wet-dry cycles, the porosity measured through MIP tests was plotted against the hydraulic conductivity values. Fig. 25a–b plots the variation of hydraulic conductivity with inter-aggregate porosity of R-B mixes during wet-dry cycles and chemical contamination, respectively.

It should be noted here that the hydraulic conductivity measured using the flexible wall apparatus at 20 kPa confining pressure is plotted in Fig. 25. The inter-aggregate porosity is calculated as intruded pores volume corresponding to pore size >4 μm captured through the MIP tests, and do not include all the inter-aggregate pores volume in the specimen due to the inability of the MIP tests to capture pore sizes >135 μm. In spite of this disadvantage, it can be observed from Fig. 25, both the hydraulic conductivity and the inter-aggregate porosity show an increasing trend with wet-dry cycles and chemical contamination. This suggests that the increase in hydraulic conductivity is directly linked to the increase in inter-aggregate porosity, owing to the pore space redistribution that occurs due to wet-dry cycles. The formation of

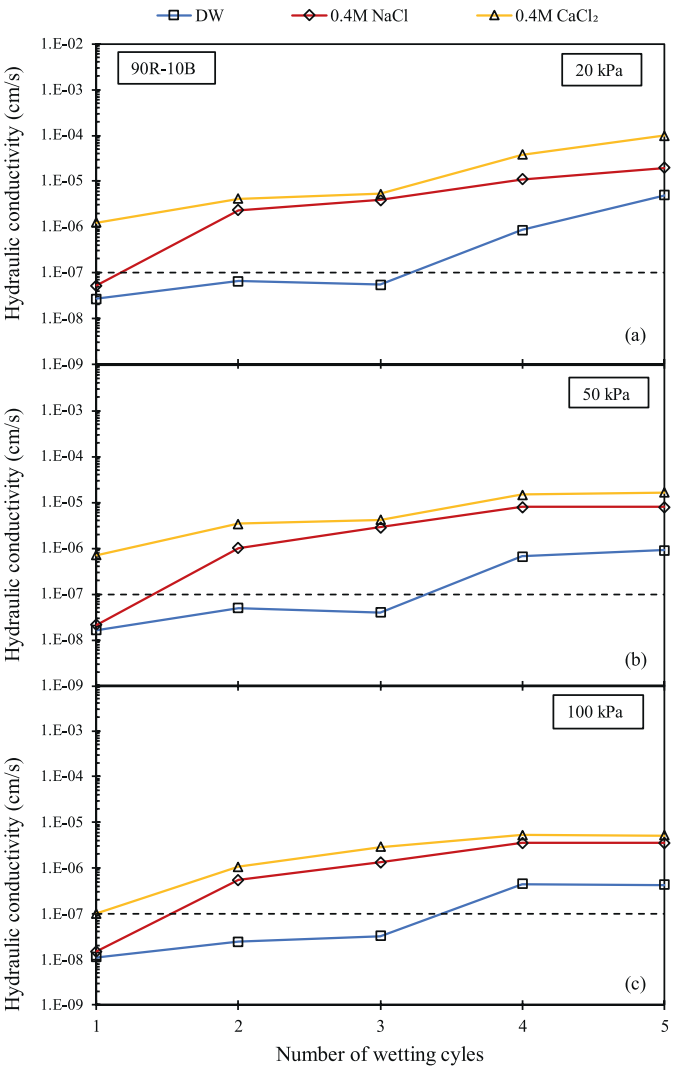

Fig. 22. Effect of wet-dry cycles and type of inundating fluid on the hydraulic conductivity of compacted 90R-10B specimen at confining pressures of (a) 20 kPa, (b) 50 kPa and (c) 100 kPa.

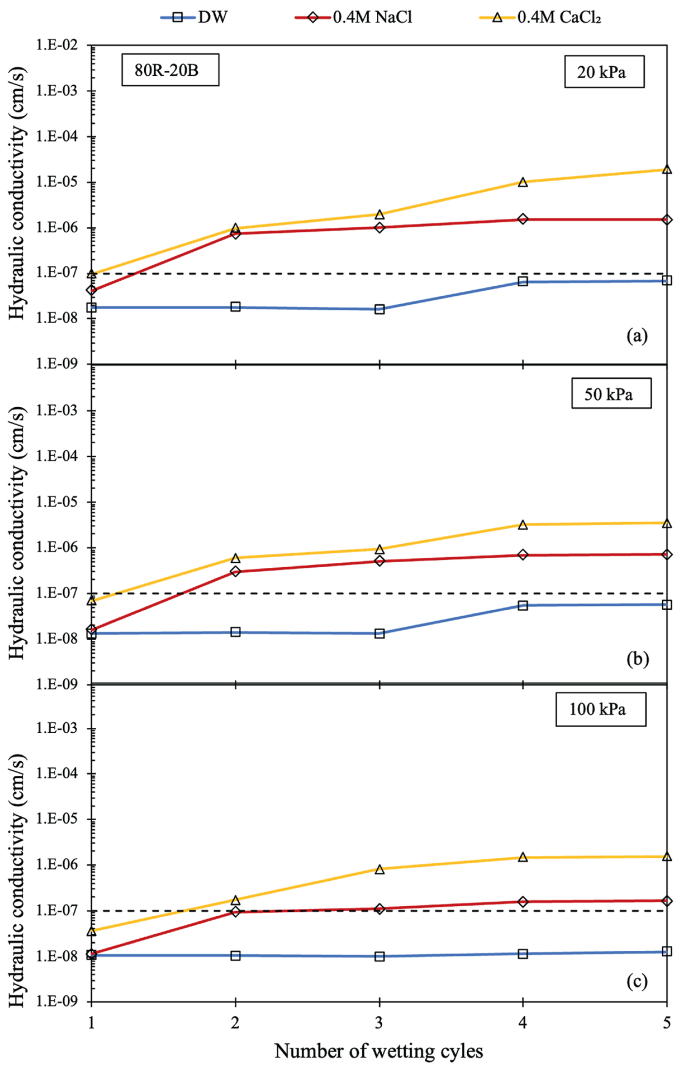

Fig. 23. Effect of wet-dry cycles and type of inundating fluid on the hydraulic conductivity of compacted 80R-20B specimen at confining pressures of (a) 20 kPa, (b) 50 kPa and (c) 100 kPa.

large interconnected flow paths within compacted clays, rather than just an increase in macropores, may further contribute to elevated hydraulic conductivity (Romero, 2013; Muddle and Briggs, 2019).

The increase in the inter-aggregate porosity and consequently the hydraulic conductivity, is more pronounced in specimens inundated with salt solutions. Since the increase in inter-aggregate porosity in R-B specimens inundated with DW resulted from the redistribution of pore sizes during the wet-dry cycles – where pores larger than 135 μm reduced in size after reaching equilibrium (Devapriya and Thyagaraj, 2024) – the corresponding increase in hydraulic conductivity is minimal for the 80R–20B and 70R–30B mixtures. Additionally, the combined effects of wet-dry cycles and induced osmotic suction become more drastic with the decrease in bentonite content in the R-B mixes.

4. Significance and future scope

The present study is especially relevant given the predicted shifts in climate patterns, which are expected to result in extended periods of both drought and heavy rainfall (IPCC et al., 2023). Such climatic variability presents substantial challenges to current landfill liner designs, highlighting the urgent need for further research. As landfill liners serve as critical geo-infrastructure for protecting public health and the environment, it is essential to understand how compacted clay liners behave under cyclic environmental loading. Furthermore, using locally sourced soils can minimize disruptions to the natural geological conditions of the area, avoiding the introduction of foreign materials that could alter the landscape. This practice also reduces construction and monitoring costs by eliminating the need to transport and manage external resources, ensuring a more sustainable integration with

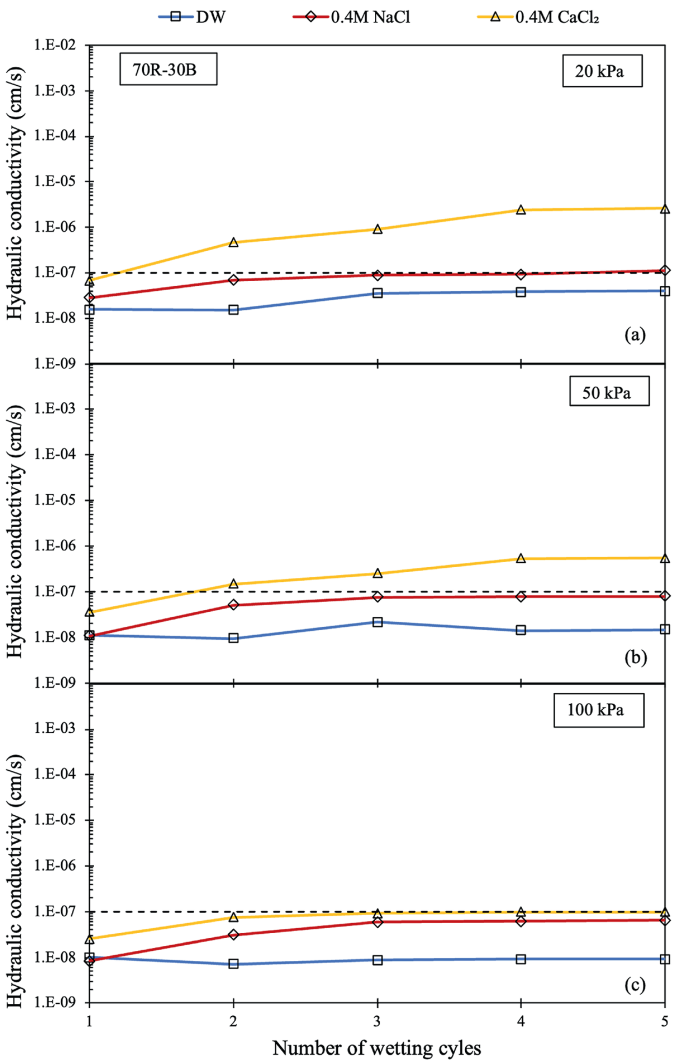

Fig. 24. Effect of wet-dry cycles and type of inundating fluid on the hydraulic conductivity of compacted 70R-30B specimen at confining pressures of (a) 20 kPa, (b) 50 kPa and (c) 100 kPa.

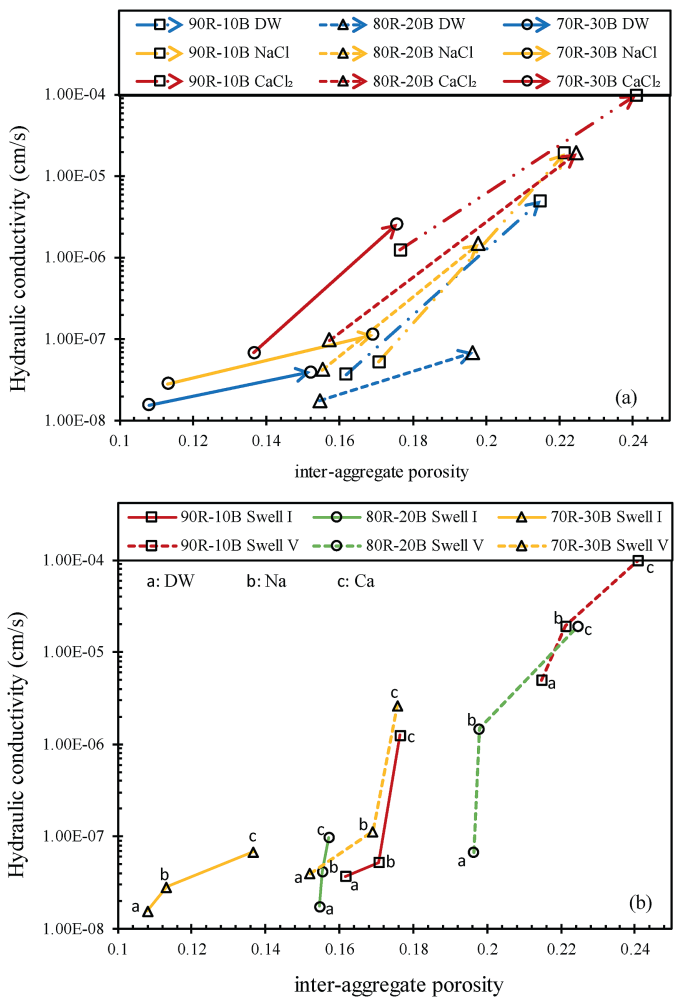

Fig. 25. Variation of hydraulic conductivity with inter-aggregate porosity of R-B mixes during (a) wet-dry cycles and (b) chemical contamination.

the natural environment onsite (Allen, 2001).

This study confirms that volume deformations in compacted soil-bentonite mixtures stabilize within five wet-dry cycles, suggesting structural equilibrium. This indicates that, under controlled conditions, further cycles may not significantly alter the soil's macroscopic behaviour. However, long-term field performance can still be influenced by factors not captured in laboratory conditions. While equilibrium in deformation suggests stability, localized effects such as microstructural rearrangements, chemical interactions, or environmental variations (e.g., temperature fluctuations, groundwater chemistry) could still play a role in extended service conditions. Future studies could investigate these aspects under prolonged cycling and field conditions to validate the long-term performance.

5. Conclusions

The present experimental studies assisted with SEM and MIP microstructural analyses and digital camera image analyses throw more light on the volume change and hydraulic behaviour of compacted R-B mixes under alternating wet-dry cycles and chemical contamination for the engineered barrier applications. The results confirm that the combined influence of cyclic wetting-drying and induced osmotic suction significantly alter the as-compacted properties, with the extent of impact being more pronounced in specimens with lower bentonite content.

While all three R-B mixes (with 10%, 20%, and 30% bentonite) satisfied the hydraulic conductivity criterion ($\leq 1 \times 10^{-7}$ cm/s) in their as-compacted state, exposure to wet-dry cycles under chemical contamination resulted in a marked increase in the hydraulic conductivity. By the end of the cycles, only the mix with 30% bentonite content retained its hydraulic performance within the required limits when inundated with salt solutions.

Microstructural analyses confirmed that the increase in osmotic suction and repeated wetting-drying led to inter-aggregate pore expansion, which governed the deterioration in hydraulic performance.

These findings underscore the necessity of assessing the long-term stability under field-representative conditions before adopting the compacted clay barriers in engineered containment applications.

CRediT authorship contribution statement

A.S. Devapriya: Writing – original draft, Validation, Investigation, Formal analysis, Data curation, Conceptualization. **T. Thyagaraj:** Writing – review & editing, Visualization, Validation, Supervision, Resources, Methodology, Conceptualization.

Declaration of competing interest

The authors declare that they have no known competing financial interests or personal relationships that could have appeared to influence the work reported in this paper.

References

Abbas, M.F., Shaker, A.A., Al-Shamrani, M.A., 2023. Hydraulic and volume change behaviors of compacted highly expansive soil under cyclic wetting and drying. J. Rock Mech. Geotech. Eng. 15 (2), 486–499.

Akgun, H., Ada, M., Kockar, M., 2015. Performance assessment of a bentonite sand mixture for nuclear waste isolation at the potential Akkuyu Nuclear Waste Disposal Site, Southern Turkey. Environ. Earth Sci. 73 (10), 6101–6116.

Albrecht, B.A., Benson, C.H., 2001. Effect of desiccation on compacted natural clays. J. Geotech. Geoenviron. Eng. ASCE 127 (1), 67–75.

Allen, A., 2001. Containment landfills: the myth of sustainability. Eng. Geol. 60 (1–4), 3–19.

Anandarajah, A., 2003. Mechanism controlling permeability change in clays due to changes in pore fluid. J. Geotech. Geoenviron. Eng. ASCE 129 (2). https://doi.org/10.1061/(ASCE)1090-0241(2003)129:2(163).

ASTM D5084-16a, 2016. Standard Test Methods for Measurement of Hydraulic Conductivity of Saturated Porous Materials Using a Flexible Wall Permeameter. ASTM International, West Conshohocken, PA, USA.

ASTM D5856-15, 2015. Standard Test Method for Measurement of Hydraulic Conductivity of Porous Material Using a rigid-wall, compaction-mould Permeameter. ASTM International, West Conshohocken, PA, USA.

ASTM D7100-11, 2020. Standard Test Method for Hydraulic Conductivity Compatibility Testing of Soils with Aqueous Solutions. ASTM International, West Conshohocken, PA, USA.

Castellanos, E., Villar, M.V., Romero, E., Lloret, A., Gens, A., 2008. Chemical impact on the hydro-mechanical behaviour of high-density FEBEX bentonite. Phys. Chem. Earth 33, S516–S526.

Chen, Y.G., Cai, Y.Q., Pan, K., Ye, W.M., Wang, Q., 2022. Influence of dry density and water salinity on the swelling pressure and hydraulic conductivity of compacted GMZ01 bentonite–sand mixtures. Acta Geotech 17 (2), 1879–1896.

Devapriya, A.S., Thyagaraj, T., 2024. Evaluation of red soil-bentonite mixtures for compacted clay liners. J. Rock Mech. Geotech. Eng. 16 (2), 697–710.

Dutta, J., Mishra, A.K., Das, P., 2018. Combined effect of inorganic salts and heavy metals on the engineering behaviour of compacted bentonites. Int. J. Geosynth. Ground Eng. 4 (17). https://doi.org/10.1007/s40891-018-0134-x.

Fu, X.L., Jiang, Z.Y., Huang, J.K., Du, Y.J., 2024. Sand-bentonite backfill amended with composite polymer exposed to organic acid: hydraulic performance and microstructural properties. J. Rock Mech. Geotech. Eng. 17 (4), 2552–2565.

Gens, A., Alonso, E.E., 1992. A framework for the behavior of unsaturated expansive clays. Can. Geotech. J. 29 (6), 1013–1032.

He, Y., Cui, Y.J., Ye, W.M., Conil, N., 2017. Effects of wetting-drying cycles on the air permeability of compacted Téguline clay. Eng. Geol. 228, 173–179.

He, Y., Ye, W.M., Chen, Y.G., Zhang, K.N., Wu, D.Y., 2020. Effects of NaCl solution on the swelling and shrinkage behavior of compacted bentonite under one-dimensional conditions. Bull. Eng. Geol. Environ. 79 (3), 399–410.

IPCC, 2023. Summary for policymakers. In: Lee, H., Romero, J. (Eds.), Climate Change 2023: Synthesis Report. Contribution of Working Groups I, II and III to the Sixth Assessment Report of the Intergovernmental Panel on Climate Change. IPCC, Geneva, Switzerland, pp. 1–34.

Julina, M., Thyagaraj, T., 2020. Combined effects of wet-dry cycles and interacting fluid on desiccation cracks and hydraulic conductivity of compacted clay. Eng. Geol. 267, 105505.

Kjeldsen, P., Barlaz, M.A., Rooker, A.P., Baun, A., Ledin, A., Christensen, T.H., 2002. Present and long-term composition of MSW landfill leachate. Crit. Rev. Environ. Sci. Technol. 32 (4), 297–336.

Li, J.S., Xue, Q., Wang, P., Liu, L., 2013. Influence of leachate pollution on mechanical properties of compacted clay: a case study on behaviors and mechanisms. Eng. Geol. 167, 128–133.

Li, J.H., Li, L., Chen, R., Li, D.Q., 2016. Cracking and vertical preferential flow through landfill clay liners. Eng. Geol. 206, 33–41.

Li, Z., Su, G., Zheng, Q., Nguyen, T.S., 2020. A dual-porosity model for the study of chemical effects on the swelling behaviour of MX-80 bentonite. Acta Geotech 15, 635–653.

Lin, L.C., Benson, C.H., 2000. Effect of wet-dry cycling on swelling and hydraulic conductivity of GCLs. J. Geotech. Geoenviron. Eng. 126 (1), 40–49.

Lin, J., Zou, W., Han, Z., Zhang, Z., Wang, X., 2022. Structural, volumetric and water retention behaviors of a compacted clay upon saline intrusion and freeze-thaw cycles. J. Rock Mech. Geotech. Eng. 14 (3), 953–966.

Lu, P.H., He, Y., Zhang, Z., Ye, W.M., 2021. Predicting chemical influence on soil water retention curves with models established based on pore structure evolution of compacted clay. Comput. Geotech. 138, 104360.

Lu, Y., Gu, K., Zhang, Y., Shen, Z., Tang, C.S., Zhou, Q., Shi, B., 2025. Biochar–water–soil interactions: implications for soil desiccation cracking behavior in subtropical regions. J. Rock Mech. Geotech. Eng. 17 (3), 1876–1888.

Mallick, S.P., Patel, H.V., Gawande, S., Wadee, A., Chen, H., McKenna, A.M., Brazil, B., Yu, W., Zhao, R., 2024. Using landfill leachate to indicate the chemical and biochemical activities in elevated temperature landfills. J. Environ. Manag. 351, 119719.

Manca, D., Ferrari, A., Laloui, L., 2016. Fabric evolution and the related swelling behaviour of a sand/bentonite mixture upon hydro-chemo-mechanical loadings. Geotechnique 66 (1), 41–57.

Mishra, A.K., Ohtsubo, M., Li, L., Higashi, T., 2005. Effect of salt concentrations on the permeability and compressibility of soil-bentonite mixtures. J. Fac. Agric. 50 (2), 37–43.

Mitchell, J.K., Soga, K., 2005. Fundamentals of Soil Behaviour, third ed. Wiley, New York.

Muddle, D.M., Briggs, K.M., 2019. Macropore structure and permeability of clay fill samples from a historic clay fill earthwork. Transp. Geotech. 19, 96–109.

Nowamooz, H., Masrouri, F., 2010. Relationships between soil fabric and suction cycles in compacted swelling soils. Eng. Geol. 114 (3), 444–455.

Ramesh, S., Thyagaraj, T., 2022. Volumetric and hydraulic behaviour of compacted natural clay–sand mixtures during wet–dry cycles. Bull. Eng. Geol. Environ. 81 (6), 241.

Rao, S.M., Thyagaraj, T., 2007. Swell–compression behaviour of compacted clays under chemical gradients. Can. Geotech. J. 44 (5), 520–532.

Rao, S.M., Thyagaraj, T., Thomas, H.R., 2006. Swelling of compacted clay under osmotic gradients. Geotechnique 56 (10), 707–713.

Razakamanantsoa, A.R., Djeran-Maigre, I., 2016. Long term chemo-hydro-mechanical behaviour of compacted soil bentonite polymer complex submitted to synthetic leachate. Waste Manag. 53, 92–104.

Romero, E., 2013. A microstructural insight into compacted clayey soils and their hydraulic properties. Eng. Geol. 165 (4), 3–19.

Sanchez, M., Gens, A., Guimaraes, L.D.N., Olivella, S., 2005. A double structure generalized plasticity model for expansive materials. Int. J. Numer. Anal. Model. 29 (8), 751–787.

Sivapullaiah, P.V., Lakshmikantha, H., 2005. Chemical compatibility of lime stabilised Indian red earth as liner material. Soil Sediment Contam. 14 (6), 515–526.

Sun, H., Mašín, D., Najser, J., Nedėla, V., Navrátilová, E., 2019. Bentonite microstructure and saturation evolution in wetting–drying cycles evaluated using ESEM, MIP and WRC measurements. Geotechnique 69 (8), 713–726.

Tan, Y., Zhou, G., Zhang, H., Li, X., Liu, P., 2024. Effect of drying cracks on swelling and self-healing of bentonite-sand blocks used as engineered barriers for radioactive waste disposal. J. Rock Mech. Geotech. Eng. 16 (5), 1776–1787.

Thyagaraj, T., Das, A.P., 2017. Physico-chemical effects on collapse behaviour of compacted red soil. Geotechnique 67 (7), 559–571.

Thyagaraj, T., Julina, M., 2019. Effect of interacting fluid and wet-dry cycles on microstructure and hydraulic conductivity of compacted clay soil. Géotech. Lett. 9 (4), 348–354.

Thyagaraj, T., Rao, S.M., 2015. Osmotic flow in compacted expansive clay. Environ. Geotech. 2 (2), 87–94.

Thyagaraj, T., Salini, U., 2015. Effect of pore fluid osmotic suction on matric and total suctions of compacted clay. Geotechnique 65 (11), 952–960.

Thyagaraj, T., Thomas, S.R., Das, A.P., 2016. Physico-chemical effects on shrinkage behavior of compacted expansive clay. Int. J. GeoMech. 17 (2). https://doi.org/10.1061/(ASCE)GM.1943-5622.0000698.
Wan, Y., Xue, Q., Liu, L., 2014. Study on the permeability evolution law and the micro-mechanism of CCL in a landfill final cover under the dry-wet cycle. Bull. Eng. Geol. Environ. 73 (4), 1089–1103.
Wang, G., Wei, X., 2015. Modelling swelling-shrinkage behaviour of compacted expansive soils during wetting–drying cycles. Can. Geotech. J. 52 (6), 783–794.
Yesiller, N., Miller, C.J., Inci, G., Yaldo, K., 2000. Desiccation and cracking behavior of three compacted landfill liner soils. Eng. Geol. 57 (1–2), 105–121.
Zhang, Z., Geng, W.S., Ye, W.M., He, Y., Su, W., Wang, Q., Chen, Y.G., 2024. Comparative study of hydro-mechanical behaviors of compacted bentonite powder and granular bentonite. J. Rock Mech. Geotech. Eng. 17 (3), 1757–1769.
Zou, W.l., Ye, J.B., Han, Z., Vanapalli, S.K., Tu, H.Y., 2018. Effect of montmorillonite content and sodium chloride solution on the residual swelling pressure of an expansive clay. Environ. Earth Sci. 77 (19), 1–12.

Dr. T. Thyagaraj is currently a professor at the Department of Civil Engineering, Indian Institute of Technology Madras, India. He obtained his BE degree (Civil) from Osmania University, Hyderabad, and MSc (Engg.) degree and PhD from Indian Institute of Science, Bangalore. He is actively engaged in teaching, research, consultancy and administration at IIT Madras. His research interests include unsaturated soil behavior, ground improvement, geoenvironmental engineering and use of waste materials in civil engineering applications. Dr. Thyagaraj received the prestigious Indian Geotechnical Society (IGS)'s Prof. Dinesh Mohan Award in 2016 for excellence in geotechnical practices. Dr. Thyagaraj is currently an active Executive Council Member of IGS National body and IGS Chennai Chapter. He has served as an Editorial Board Member of International Journal of Geotechnical Engineering and Indian Geotechnical Journal. Currently, he is serving as an Editorial Board Member of Scientific Reports.